Bioresource Technology 330 (2021) 125002

Contents lists available at ScienceDirect

Bioresource Technology

journal homepage: www.elsevier.com/locate/biortech

Metabolic alteration of *Methylococcus capsulatus* str. Bath during a microbial gas-phase reaction

Yan-Yu Chen [a,1], Yuki Soma [b,1], Masahito Ishikawa [a,c,1], Masatomo Takahashi [b], Yoshihiro Izumi [b], Takeshi Bamba [b], Katsutoshi Hori [a,*]

[a] Department of Biomolecular Engineering, Graduate School of Engineering, Nagoya University, Furo-cho, Chikusa-ku, Nagoya 464-8603, Japan
[b] Division of Metabolomics, Medical Institute of Bioregulation, Kyushu University, Higashi-ku, Fukuoka 812-8582, Japan
[c] PRESTO, Japan Science and Technology Agency, 4-1-8 Honcho, Kawaguchi, Saitama 332-0012, Japan

HIGHLIGHTS

- A gas-phase reactor was constructed for comparative metabolome analysis.
- Efficient methane degradation by *M. capsulatus* proceeds in the gas-phase reactor.
- Remarkable alterations occur in the metabolism of cells in the gas-phase reaction.
- 2-Ketoglutarate was accumulated in *M. capsulatus* due to high methane availability.
- Useful products such as xanthines were accumulated during the gas-phase reaction.

GRAPHICAL ABSTRACT

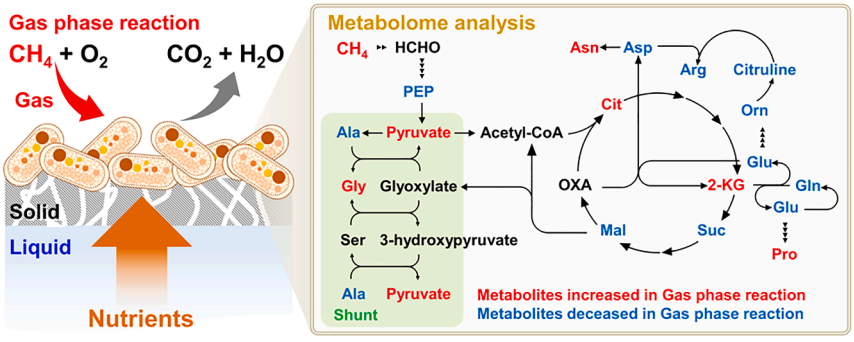

ARTICLE INFO

Keywords:
Methane
Methanotroph
Metabolome analysis
Microbial gas-phase reaction
Methylococcus capsulatus (Bath)

ABSTRACT

This study demonstrates the metabolic alteration of *Methylococcus capsulatus* (Bath), a representative bacterium among methanotrophs, in microbial gas-phase reactions. For comparative metabolome analysis, a bioreactor was designed to be capable of supplying gaseous substrates and liquid nutrients continuously. Methane degradation by *M. capsulatus* (Bath) was more efficient in a gas-phase reaction operated in the bioreactor than in an aqueous phase reaction operated in a batch reactor. Metabolome analysis revealed remarkable alterations in the metabolism of cells in the gas-phase reaction; in particular, pyruvate, 2-ketoglutarate, some amino acids, xanthine, and hypoxanthine were accumulated, whereas 2,6-diaminopimelate was decreased. Based on the results of metabolome analysis, cells in the gas-phase reaction seemed to alter their metabolism to reduce the excess ATP and NADH generated upon increased availability of methane and oxygen. Our findings will facilitate the development of efficient processes for methane-based bioproduction with low energy consumption.

* Corresponding author.
E-mail address: khori@chembio.nagoya-u.ac.jp (K. Hori).
[1] These authors contributed equally to this work.

https://doi.org/10.1016/j.biortech.2021.125002
Received 11 February 2021; Received in revised form 9 March 2021; Accepted 10 March 2021
Available online 16 March 2021

1. Introduction

Methane (CH_4), the main component of natural gas, biogas, and shale gas, has been used as a significant energy source for a long time. In the past decade, its abundance and relatively low price have made CH_4 a promising next-generation carbon feedstock (Fei et al., 2014). Nevertheless, the use of CH_4 as a carbon feedstock is still limited because its conversion is hindered by an extremely stable C–H bound (440 kJ/mol of the dissociation energy of the C–H bond) (Bjorck et al., 2018). Although the conversion of CH_4 with chemical catalysts has been studied extensively, most of the reactions involved are energy intensive and ecologically unfriendly (Wang et al., 2017).

Methanotrophs, a group of microorganisms, utilize CH_4 as the sole carbon and energy source, with their unique enzymes and metabolic pathways (Cantera et al., 2019). This property of methanotrophs allows them to be used as biocatalysts for the conversion of CH_4 into valuable products at ordinary temperature and pressure, supporting the development of green bioprocesses. Many methanotrophic bioprocesses have been applied to obtain various products, such as methanol (Patel et al., 2020a, 2020b), polyhydroxyalkanoates (Pieja et al., 2011; Strong et al., 2016), single-cell proteins (Petersen et al., 2017; Zha et al., 2021), liquid biofuels (Furutani et al., 2014), succinic acid (Subbian, 2017), and isoprenoids (Jeon et al., 2019). Even though additional market-valuable products could be synthesized, methanotrophic bioprocesses still face multiple challenges. For instance, the low water solubility of CH_4 and oxygen (O_2) is one of the major factors limiting the development of industrial processes (Bjorck et al., 2018). Typical methanotrophic bioprocesses are conducted with suspended cells in an aqueous solution. Hence, vigorous agitation in the form of bubbling or stirring is required to dissolve CH_4 and O_2 into the aqueous phase to supply them to methanotrophic cells, resulting in high energy consumption.

Microbial gas-phase reactions have been proposed to enhance the rate of mass transfer of gaseous substrates from the gas phase to biocatalysts, especially for hydrophobic gases (e.g., CH_4 and O_2) (Kulishova & Zharkov, 2017; Webb, 2017). Unlike in typical bioreactions in aqueous solutions, for gas-phase reactions biocatalysts are immobilized on solid supports in the absence of an aqueous solution as a suspension medium. The removal of the aqueous solution allows biocatalysts to directly contact hydrophobic gases, and mediate biocatalytic reactions in the gas phase. Without the need for vigorous agitation, gaseous substrates can be driven by a small pressure drop or be supplied in a passive way with low energy consumption. With these perspectives, microbial gas-phase reactions have attracted the researchers' attention for the development of green processes (Kumar et al., 2021; Lamare et al., 2004; Usami et al., 2020). In a previous study, we evaluated the ability of *Methylococcus capsulatus* (Bath), a representative gamma-proteobacterial methanotroph (Ward et al., 2004), to degrade CH_4 in microbial gas-phase reactions. Notably, the rate of CH_4 degradation in a gas-phase reaction without active supply of gases was much higher than that in an aqueous phase reaction, with stirring (Chen et al., 2020). This increase in the rate of CH_4 degradation upon improved availability of gaseous CH_4 and O_2 implies that the metabolism of *M. capsulatus* (Bath) in a microbial gas-phase reaction is quite different from that in the aqueous phase reaction. Metabolome analysis would lead to a definitive understanding of the cellular states, the rate-limiting steps of metabolic flow, and the potential metabolite productivity of microbial gas-phase reactions. Limited information about the metabolome of microorganisms in microbial gas-phase reactions is available, although this could be beneficial for the development of CH_4-based green bioprocesses.

In this study, we for the first time investigated the metabolome of *M. capsulatus* (Bath) in the microbial gas-phase reaction. For comparative metabolome analysis with typical aqueous phase reactions, a bioreactor for the gas-phase reaction was constructed, which can continuously supply gas substrates and liquid nutrients unlike a batch bioreactor used in the previous study (Chen et al., 2020). Methane degradation by *M. capsulatus* (Bath) in a gas-phase reaction operated in the constructed reactor was evaluated and compared with that in an aqueous phase reaction. The metabolome of *M. capsulatus* (Bath) during the gas-phase reaction was compared with that in the aqueous phase reaction.

2. Materials and methods

2.1. Cultivation of Methylococcus capsulatus (Bath)

M. capsulatus (Bath) was cultivated in a 5 L flask containing 1 L of nitrate mineral salt (NMS) medium (pH 6.8) consisting of 1.0 g of KNO_3, 1.0 g of $MgSO_4{\cdot}7H_2O$, 0.2 g of $CaCl_2{\cdot}2H_2O$, 0.497 g of Na_2HPO_4, 0.39 g of KH_2PO_4, 0.019 g of Fe-EDTA, 0.0005 g of $Na_2MoO_4{\cdot}2H_2O$, and 0.1 mL of trace element solution per liter of distilled water, incubated with 20 μM $CuCl_2$ at 42 °C with stirring for 5 d. The trace element solution contains 0.5 g of $FeSO_4{\cdot}7H_2O$, 0.4 g of $ZnSO_4{\cdot}7H_2O$, 0.25 of Na_2EDTA, 0.015 g of H_3BO_3, 0.05 g of $CoCl_2{\cdot}6H_2O$, 0.02 g of $MnCl_2{\cdot}4H_2O$, and 0.01 g of $NiCl_2{\cdot}6H_2O$ per 100 mL of distilled water. CH_4 and air were supplied by bubbling and passive diffusion from 1-L rubber balloons, respectively. Cells were harvested by centrifugation at 6,000 rpm for 20 min, washed three times with freshly sterilized NMS medium containing 20 μM $CuCl_2$, and resuspended in the same medium for further experiments.

2.2. Aqueous phase reaction in a batch vial

Ten milligrams of dry cell weight (DCW) of *M. capsulatus* (Bath) cells were suspended in 5 mL of NMS medium with 20 μM $CuCl_2$ and infused into a 30 mL sterilized cylindrical glass vial. The vial was then sealed with a sterilized rubber plug and an aluminum cap. Pure CH_4 was injected into the vial with a gas-tight syringe to achieve a final CH_4 concentration of 20% in the headspace of the vial. Vials without cells were prepared as controls using the same procedure. Reactions were performed at 42 °C for 3 h with shaking at 140 rpm. The concentration of CH_4 in the headspace was measured at 0.5-h intervals by gas chromatography, as described previously (Chen et al., 2020).

2.3. Gas-phase reaction in a continuous bioreactor

For the gas-phase reaction, a bioreactor was devised to continuously supply the mixture of CH_4 and air. The following components were assembled in the bioreactor from top to bottom: a sandwich structure: a polycarbonate (PC) gas chamber, a polytetrafluoroethylene (PTFE) gasket, a glass fiber filter with immobilized cells, a PC filter support, and a PC liquid chamber. These components were then locked tightly using screws and nuts. All the components were treated with UV light on a clean bench for 30 min before assembly. *M. capsulatus* (Bath) cells were immobilized by filtration on a sterilized glass fiber filter with a diameter of 47 mm (GF/F 47; GE Healthcare), which was then assembled into the center of the bioreactor. The side of the filter with immobilized cells was placed facing the top of the gas chamber, whereas the other side of the filter was in contact with the liquid phase in the bottom of the chamber. The liquid chamber and gas chamber were 40 mm in diameter and 2 mm in height, resulting in a volume of 2.5 mL. A reaction solution consisting of 10 mL of NMS medium with 20 μM $CuCl_2$ was infused into the liquid chamber and circulated between the solution container and the liquid chamber by a peristaltic pump (ISM931; ISMATEC) at a rate of 3 mL/min. For supplying gaseous substrates, a mixture of CH_4 and air (80% N_2 and 20% O_2) at a ratio of 1:4 was prepared by a gas blender (BR-2CS; KOFLOC Kyoto) and injected continuously into the gas chamber. To optimize cell concentration in the bioreactor, 1, 4, 7, 10, 15, 20, and 25 mg-DCW of *M. capsulatus* (Bath) cells were prepared and immobilized on the glass fiber filter. The gas flow rate was set at 10 mL/min with a 20% CH_4 concentration for 10 min, to purge the air in the gas chamber, and then changed to 1 mL/min for 170 min. Reactions were performed at 42 °C by incubating a bioreactor in a water bath. CH_4 concentration was

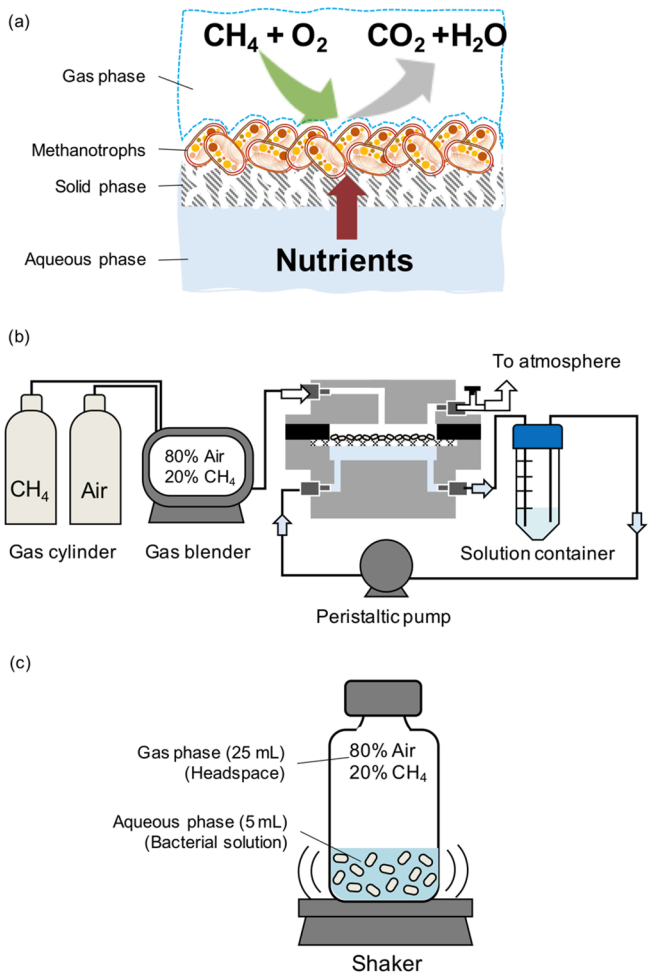

Fig. 1. Illustrations of systems for the gas-phase reaction and the aqueous phase reaction. (a) Conceptual design of a reactor capable of supplying gaseous substrates (CH_4 and O_2) and liquid nutrients continuously. (b) Configuration of the system for the gas-phase reaction. (c) Batch-type vial system for the aqueous phase reaction.

analyzed by sampling the gas at the outlet at 0.5 h intervals. To determine the CH_4 removal rate, the difference in CH_4 concentrations between the inlet and the outlet was multiplied by the volumetric gas flow rate, divided by the volume of the gas chamber, and then converted to g-CH_4/(L-gas phase·h) according to the ideal gas law at 1 atm and 42 °C.

2.4. Metabolomic analysis

Cultured cells of *M. capsulatus* (Bath) were divided into 6 sets: 3 sets for performing aqueous phase reactions and 3 sets for performing gas-phase reactions. The cells were washed with fresh sterilized NMS medium containing 20 μM $CuCl_2$, resuspended in the same medium, and utilized for aqueous or gas-phase reactions. After 3 h of incubation, the cells were harvested for metabolome analysis as follows. For samples in the aqueous phase reaction, 5 mL of the cell suspension in each of the vials was filtered through a hydrophilic 0.45-μm PTFE membrane filter of 47 mm in diameter (Omnipore Membrane Filters, Millipore, JHWP04700) on a filtration system. For gas-phase reaction samples, the glass fiber filter with the immobilized cells was removed from the bioreactor and then set on the filtration system. Aqueous phase and gas-phase reaction samples on the filters were washed with 10 mL of 110 mM ammonium acetate, flash-frozen in liquid nitrogen, desiccated by freeze-drying overnight, and stored at –80 °C before metabolome analysis.

Cells attached to each collecting filter were peeled off and lysed with 2 mL of ice-cold methanol in a 50 mL conical tube and vortexed for 1 min. After flash centrifugation to spin down the filtrate and the solution, each tube was wrapped with aluminum foil and its content subjected to ultrasonic disruption for 5 min. After flash centrifugation, the tubes were placed in a −20 °C freezer for 1 h. After removal of the filters from conical tubes, the tubes were centrifuged at 16,000 × *g* for 5 min. Each 600 μL of the cell lysate supernatant was diluted with 600 μL of chloroform and 480 μL of water. The samples were centrifuged again at 16,000 × *g* for 5 min. The top phase (850 μL) was collected and evaporated to dryness using a centrifugal concentrator (VC-36S, TAITEC). Prior to analysis, the dried aqueous layer was reconstituted in 50 μL of water containing 10 μM 10-camphorsulfonic acid and 10 μM 1,4-piperazinediethanesulfonic acid (PIPES) as internal standards, resulting in an analytical sample for metabolomic analysis.

Anionic polar metabolites (i.e., organic acids, sugar phosphates, nucleotides, etc.) were analyzed via ion chromatography (Dionex ICS-5000$^+$ HPIC system, Thermo Fisher Scientific) with a Dionex IonPac AS11-HC-4 μm column (2 mm i.d. × 250 mm, 4 μm particle size, Thermo Fisher Scientific) coupled with a Q Exactive, high-performance benchtop quadrupole Orbitrap high-resolution tandem mass spectrometer (Thermo Fisher Scientific) (IC/HRMS/MS) (Fushimi et al., 2020; Izumi et al., 2019). Cationic polar metabolites (i.e., amino acids, bases, nucleosides, etc.) were analyzed via liquid chromatography (Nexera X2 UHPLC system, Shimadzu) with a Discovery HS F5 column (2.1 mm i.d. × 150 mm, 3 μm particle size, Merck) coupled with a Q Exactive instrument (PFPP-LC/HRMS/MS) (Fushimi et al., 2020; Izumi et al., 2019).

3. Results and discussion

3.1. Development of a bioreactor for microbial gas-phase reactions

In a previous study, we demonstrated rapid CH_4 degradation by *M. capsulatus* (Bath) in a microbial gas-phase reaction with a batch bioreactor (Chen et al., 2020). However, this batch system is not suitable for comparative metabolome analysis because liquid nutrients cannot be supplied sustainably. In this study, we developed a bioreactor for microbial gas-phase reactions, which can supply gaseous substrates (CH_4 and O_2) and liquid nutrients continuously. The design concept of the reactor is shown in Fig. 1a. The biofilm of *M. capsulatus* (Bath), immobilized on a porous solid material, was proposed to be placed in contact with a gas phase but not immersed in an aqueous phase; this would enable direct contact between cells and gaseous substrates without a huge water barrier, and thus enhance the efficiency of mass transfer from gaseous substrates to the cells. The nutrients dissolved in the reaction solution would be supplied to cells through the aqueous phase. The new reactor (hereafter called GPR, the abbreviation of gas-phase reactor) was assembled as a sandwich structure in the middle of which a glass fiber filter with immobilized *M. capsulatus* (Bath) cells was set, separating the gas phase and the aqueous phase into an upper and lower chamber, respectively (Fig. 1b). Although one side of the filter was still connected to the solution in the aqueous phase, the negative pressure generated by the peristaltic pump for liquid circulation withdrew the water from the filter. Therefore, the biofilm on the filter could be maintained in a semi-dry state while nutrients in the medium could still be supplied to the biofilm by diffusion.

To achieve rapid CH_4 degradation by a microbial gas-phase reaction in the assembled GPR, the effect of the concentration of *M. capsulatus* (Bath) cells on the removal rate of CH_4 in the GPR was investigated. Different amounts of *M. capsulatus* (Bath) cells were prepared and immobilized on the glass fiber membrane acting as a support. The cell amount in DCW was normalized by the volume of the glass fiber membrane (0.72 mL), resulting in 1.4, 5.6, 9.7, 13.9, 20.8, 27.8 and 34.7 g-DCW/L-support. When air supplemented with 20% (v/v) of CH_4 at a total gas flow rate of 1 mL/min was used as inlet gas, the removal

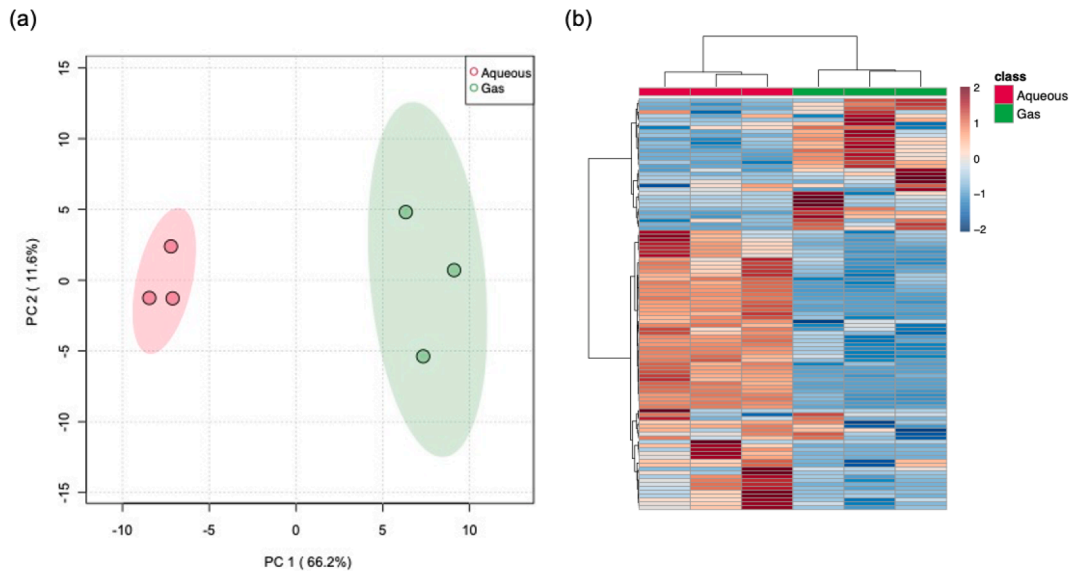

Fig. 2. (a) Principal component analysis and (b) hierarchical cluster analysis of 105 metabolites detected in *Methylococcus capsulatus* (Bath) cells catalyzing aqueous phase and gas-phase reactions for 3 h. PC1 and PC2 indicate first and second principal component scores, respectively. The numbers in the parentheses show the contributing ratio of each score.

rate of CH_4 increased linearly with cell concentration, starting at 0.08 g-CH_4/(L-gas phase·h) and then reaching up to 0.36 g-CH_4/(L-gas phase·h), until a cell concentration of 13.9 g-DCW/L-support, but became constant at higher cell concentrations. This result suggests that the resistance of mass transfer due to biofilm thickness limits the increase in the removal rate of CH_4 at high cell concentrations. For effective CH_4 degradation in further experiments, the immobilized cell amount was optimized to 10 mg-DCW (13.9 g-DCW/L-support).

When investigating the effect of the gas flow rate on the removal rate of CH_4 in the GPR, we observed no significant difference in removal rate in the range from 0.25 mL/min to 1.5 mL/min (data not shown). At gas flow rates higher than 2.0 mL/min, the CH_4 removal rate fell below the detection limit because the concentration of CH_4 at the outlet became almost the same as that at the inlet, indicating that at a flow rate above 2.0 mL/min the retention time was too short to allow conversion of CH_4 in the assembled GPR.

3.2. Comparison of methane degradation: gas-phase reaction in the gas-phase reactor versus aqueous phase reaction in a batch reactor

Using the optimized conditions, the efficiency of CH_4 degradation in the GPR (gas-phase reaction) was compared to that in a batch reactor (aqueous phase reaction) as shown in Fig. 1c. The same amount of *M. capsulatus* (Bath) cells (10 mg-DCW) was used in both reactors. The inlet gas sample consisted of 20% (v/v) CH_4 in air pumping into a GPR at a flow rate of 1 mL/min, whereas the initial concentration of CH_4 was set at 20% (v/v) in the headspace of the vial. The efficiency of CH_4 degradation in each system was evaluated by measuring the variation in CH_4 concentration at the outlet of the GPR or the headspace of the vial over time. The concentration of CH_4 at the outlet of the GPR decreased rapidly from 20.0% to 18.0% in the first 30 min of reaction and then remained constant at 17.5% after 1 h, indicating that an excess amount of CH_4 still surrounded the methanotrophic cells. In the absence of cells, the concentration of CH_4 did not decrease in the GPR. By integrating the shaded areas in the graph presenting the time course of CH_4 concentration at the outlet of a GPR during the gas-phase reactions, the cumulative amount of degraded CH_4 was calculated to be 3.4 ± 0.2 mL during a 3 h continuous operation. On the other hands, in the vial for the aqueous phase reaction, the concentration of CH_4 in the headspace consistently decreased from 20.0% to 13.8% after 3 h. Based on the difference in CH_4 concentration between the starting point and the endpoint, the overall amount of degraded CH_4 in the vial during the 3 h batch operation was calculated to be 1.6 ± 0.1 mL, which amounted to only 47% of the volume degraded in the GPR.

The removal rates of CH_4 in two systems were calculated from the time courses of the cumulative amounts of degraded CH_4. The removal rate of CH_4 in the GPR was 0.37 ± 0.01 g-CH_4/(L-gas phase·h), which was not only about 30-fold higher than that in the batch reactor [0.013 ± 0.001 g-CH_4/(L-gas phase·h)], but also much higher than that in conventional biofiltration systems (Ganendra et al., 2015; Park et al., 2009). In the GPR, *M. capsulatus* (Bath) cells degraded CH_4 rapidly as they were in a specific environment with high carbon availability and high O_2 tension in the absence of a water barrier around cells. Hence, the cellular status of *M. capsulatus* (Bath) in the microbial gas-phase reaction was thought to be different from that assumed in a typical aqueous phase reaction.

3.3. Metabolomic analysis of M. capsulatus (Bath) cells in the microbial gas-phase reaction

To understand the metabolic status of *M. capsulatus* (Bath) cells in the microbial gas-phase reaction, the cultured cells were divided into two fractions of the same volume. One fraction was immobilized onto the surface of a filter for the microbial gas-phase reaction, and the other was resuspended in NMS medium for the aqueous phase reaction. After each reaction was carried out for 3 h, metabolites were extracted and quantified by IC/HRMS/MS and PFPP-LC/HRMS/MS. As a result, 105 metabolites were identified. Principal component analysis revealed that PC1 (horizontal axis) distinctly separated the samples of the microbial gas-phase reactions from the samples of the aqueous phase reactions (Fig. 2a). PC2 (vertical axis) clarified the differences between samples of the same group. Hierarchical cluster analysis revealed distinct metabolic patterns between cells catalyzing gas-phase reactions and those catalyzing aqueous phase reactions, indicating that the metabolic status of *M. capsulatus* (Bath) cells in the gas-phase reaction was different from that in the aqueous phase reaction (Fig. 2b). The metabolic alterations occurring in the gas-phase reaction are presented in Fig. 3. The levels of most metabolites involved in central carbon metabolism were decreased

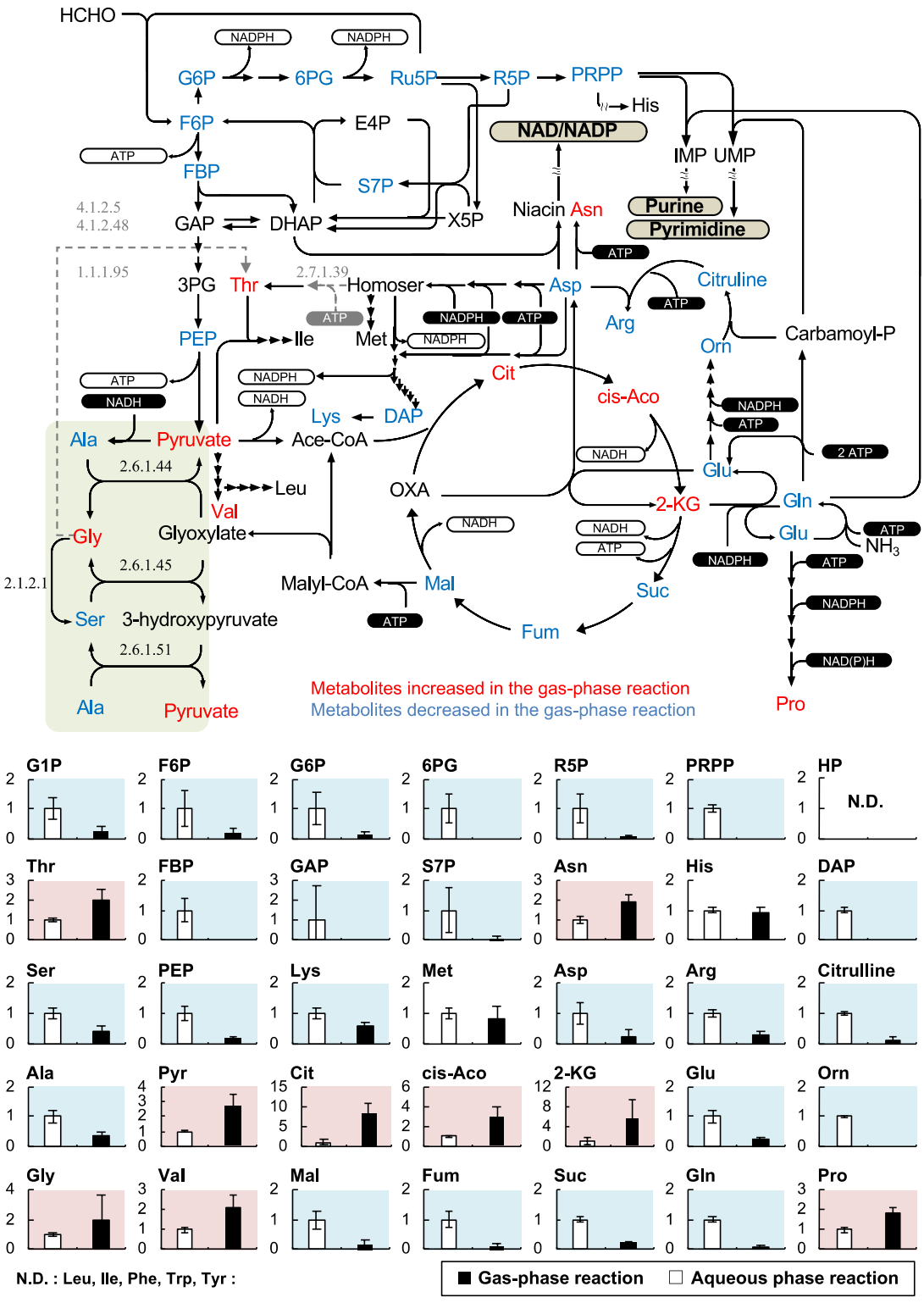

Fig. 3. Upper panel: graphical explanation of altered metabolism of *Methylococcus capsulatus* (Bath) during the gas-phase reaction within the gas-phase reactor. The putative metabolic map illustrating the possible reason for increased or decreased accumulation of certain metabolites in cells in the gas-phase reaction is highlighted by a green box; this incomplete serine cycle was considered as a pyruvate recycle shunt consuming NADH. Lower panels: each graph indicates the relative level of every detected intracellular metabolite in the gas-phase reaction normalized to its level in cells catalyzing the aqueous phase reaction for 3 h. The name of each metabolite has been abbreviated as follows: G1P, D-Glucose 1-phosphate; F6P, D-fructose 6-phosphate; G6P, D-glucose 6-phosphate; 6PG, 6-phosphogluconic acid; R5P, D-ribose 5-phosphate; PRPP, phosphoribosyl pyrophosphate; HP, 3-hydroxypyruvate; Thr, threonine; FBP, D-fructose 1,6-bisphosphate; GAP, glyceraldehyde 3-phosphate; S7P, D-sedoheptulose 7-phosphate; Asn, asparagine; His, histidine; DAP, 2,6-diaminopimelate; Ser, serine; PEP, phosphoenolpyruvate; Lys, lysine; Met, methionine; Asp, asparate; Arg, arginine; Ala, alanine; Pyr, Pyruvate; Cit, citrate; *cis*-Aco, *cis*-aconitic acid, 2-KG, 2-ketoglutarate; Orn, ornithine; Glu, glutamate; Gly, glycine; Val, valine; Mal, malate; Fum, fumarate; Suc, succinate; Gln, glutamine; and Pro, proline . Error bars show the standard deviation (n = 3).

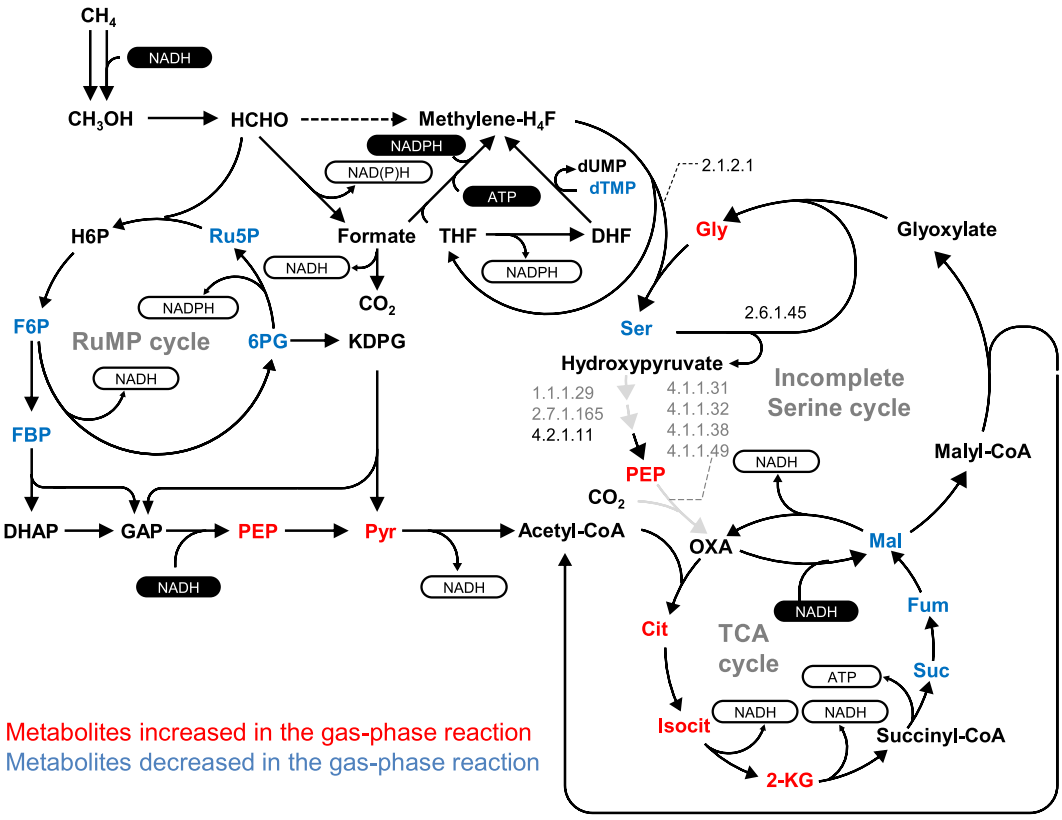

Fig. 4. Traditional overview of the central carbon metabolism of *Methylococcus capsulatus* (Bath). The central carbon metabolism of *M. capsulatus* (Bath) was described as being limited to the RuMP cycle, the TCA cycle, and an incomplete serine cycle.

in cells catalyzing gas-phase reactions, except for three metabolites: pyruvate (Pyr), citrate (Cit), and 2-ketoglutarate (2-KG). Conversely, the levels of succinate (Suc), fumarate (Fum), and glutamate (Glu), which are metabolites downstream of 2-KG, significantly decreased in the cells catalyzing gas-phase reactions.

2-KG is not only used as the major carbon skeleton in nitrogen assimilatory reactions, but also plays a role as an important signaling molecule for regulating metabolic pathways (Huergo & Dixon, 2015). Research in *Escherichia coli* has provided a better understanding of the biological role of 2-KG. The intracellular levels of 2-KG are sensitive to variations in the carbon supply: indeed, when glucose was added to cultures of *E. coli* incubated in carbon-starved conditions, the intracellular levels of 2-KG significantly increased (Chen et al., 2014; Zhang et al., 2013; Zhang & Ye, 2014). The gas-phase reaction enhances the mass transfer of CH_4 to *M. capsulatus* (Bath) cells due to the high molecular diffusion rate in a gas phase (Chen et al., 2020). The higher level of 2-KG in cells in the gas-phase reaction (Fig. 3) thus possibly reflects higher availability of CH_4 than that in the aqueous phase reaction. The consequent increase in carbon availability caused relative nitrogen depletion, resulting in a decrease in the level of glutamine (Gln). Since the lower level of Gln decelerated Glu synthesis from 2-KG, Gln, and NADPH (EC 1.4.1.13) (Rabinowitz & Silhavy, 2013), 2-KG was assumed to accumulate in cells in the gas-phase reaction. 2-KG is also known to regulate cyclic AMP synthesis by inhibiting adenylate cyclase, a master signaling molecule in *E. coli* (Daniel & Danchin, 1986; Doucette et al., 2011; You et al., 2013). Therefore, the high level of 2-KG induced by the efficient supply of CH_4 might be one of the main factors for the altered activity of metabolic pathways in cells in the gas-phase reaction. Consequently, setting cells in an GPR for gas-phase reaction could be a method to regulate their metabolism by altering the intracellular 2-KG level without the use of genetic manipulation.

Metabolome analysis enabled the detection of 13 amino acids, revealing the accumulation of asparagine (Asn), proline (Pro), glycine (Gly), valine (Val), and threonine (Thr) in cells in the gas-phase reaction (Fig. 3). Asn and Pro are end products in *M. capsulatus* (Bath), and both require ATP and/or NADPH for *de novo* synthesis. In the gas-phase reaction, the levels of the precursors of Asn and Pro, aspartic acid (Asp) and Glu, were decreased significantly in *M. capsulatus* (Bath) cells. These suggest that Asp and Glu were converted to Asn and Pro respectively with consuming ATP. The Thr biosynthetic pathway, branching from Asp, also requires ATP and NADPH, although a gene coding for homoserine kinase (EC 2.7.1.39) has not yet been identified in the genome of *M. capsulatus* (Bath). The altered levels of these amino acids suggest that in cells in the gas-phase reaction, metabolic states might be altered to reduce the excess ATP and NADPH generated upon high availability of CH_4 and O_2. *M. capsulatus* (Bath) is thought to utilize ribulose monophosphate (RuMP) and an incomplete serine cycle for formaldehyde assimilation (Fig. 4) (Gupta et al., 2019; Lee et al., 2016; Ward et al., 2004). However, the activity of this metabolic pathway cannot explain the accumulation of Gly and the decrease of Ser in absence of a significant accumulation of hydroxypyruvate. We propose that cells in the gas-phase reaction undergo a metabolic shunt, as shown in the highlighted part of Fig. 3. In this metabolic shunt, Gly and Val synthesis branch from pyruvate. Two synthetic pathways, mediated by alanine: glyoxylate aminotransferase (EC 2.6.1.44) and L-serine:glyoxylate aminotransferase (EC 2.6.1.45) and requiring Ala and Ser as the respective precursor, lead to pyruvate synthesis. Together with L-serine: pyruvate aminotransferase (EC 2.6.1.51), this shunt seizes the metabolic

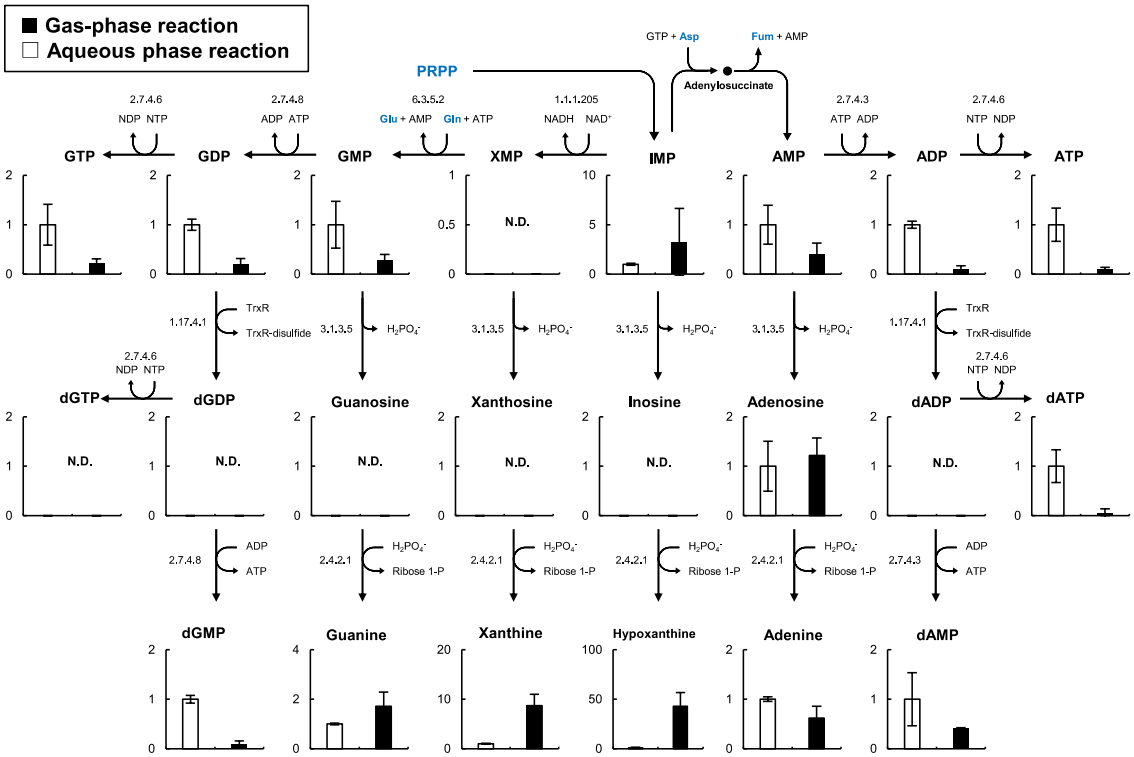

Fig. 5. Altered accumulation of metabolites involved in purine metabolism in cells in the gas-phase reaction. Each graph indicates the relative level of each intracellular metabolite normalized to the value in cells catalyzing the aqueous phase reaction for 3 h. Error bars show the standard deviation (n = 3).

flux toward Gly and pyruvate synthesis, consuming NADH via alanine dehydrogenase (EC 1.4.1.1). Since *M. capsulatus* (Bath) has no lactate dehydrogenase, which is the major metabolic enzyme for consuming excess NADH generated through glycolysis and the TCA cycle, this metabolic switch might function as an alternative to maintain the intracellular redox balance in cells in the gas-phase reaction.

The pathways involved in purine and pyrimidine metabolism are summarized in Figs. 5 and 6. The levels of most of the related metabolites were decreased significantly in cells in the gas-phase reaction, possibly due to the decreasing levels of their precursors: Gln, Glu, Asp, and phosphoribosyl pyrophosphate (PRPP) (Figs. 5 and 6). Of note, the levels of xanthine and hypoxanthine increased drastically in cells in the gas-phase reaction (Fig. 5). The production of inosine monophosphate (IMP) is the first branching point for synthesis of other purine compounds. AMP and GMP synthesis from IMP require Asp and Gln, respectively. Therefore, depletion of Gln and Asp might limit the metabolic flux toward purine synthesis, except for the pathway leading to xanthine and hypoxanthine. The derivatives of xanthine and hypoxanthine have been studied for a long time in the food and pharmaceutical industries due to their biological activities. Their efficient bioproduction from glucose has been accomplished using metabolically engineered microbes (Liu et al., 2020; McKeague et al., 2016). Our metabolome analysis suggests the feasibility of CH_4-based bioproduction of xanthine, hypoxanthine, and their derivatives by gas-phase reaction, which has not been reported so far.

The gas-phase reaction was likely to also affect the growth of *M. capsulatus* (Bath). In fact, the level of 2,6-diaminopimelate (DAP), a key molecule for the construction of the cell wall, which is essential for cell growth, was drastically decreased in cells in the gas-phase reaction (Fig. 3), suggesting the cessation of cell growth and the preference for CH_4 catabolism rather than biomass formation. This phenotype is suitable for efficient bioproduction. Indeed, for most valuable compounds, bioproduction is coupled with cell growth, although biomass formation consumes a large part of the carbon source. To address this problem, efficient bioprocesses that decouple cell growth and production have been developed using metabolic engineering approaches (David et al., 2016; Gupta et al., 2017; Soma et al., 2017, 2014; Soma & Hanai, 2015; Zhao et al., 2018). We anticipate that the use of microbial gas-phase reactions within GPRs will contribute to the development of such processes without the need for genetic manipulations.

4. Conclusion

This study is the first to demonstrate the metabolic alteration of *M. capsulatus* (Bath) in a gas-phase reaction. The gas-phase reaction operated in the GPR improved the methane degradation rate, which was about 30-fold higher than that in an aqueous phase reaction, and triggered remarkable alterations in the metabolism of cells in the gas-phase reaction. The decrease and the accumulation of some metabolites such as DAP, 2-ketoglutarate, xanthine, hypoxanthine, and their derivatives suggest the feasibility of CH_4-based bioproduction in a GPR without genetic manipulations. Our findings will contribute to the development of green processes for CH_4-based bioproduction.

Declaration of Competing Interest

The authors declare that they have no known competing financial interests or personal relationships that could have appeared to influence the work reported in this paper.

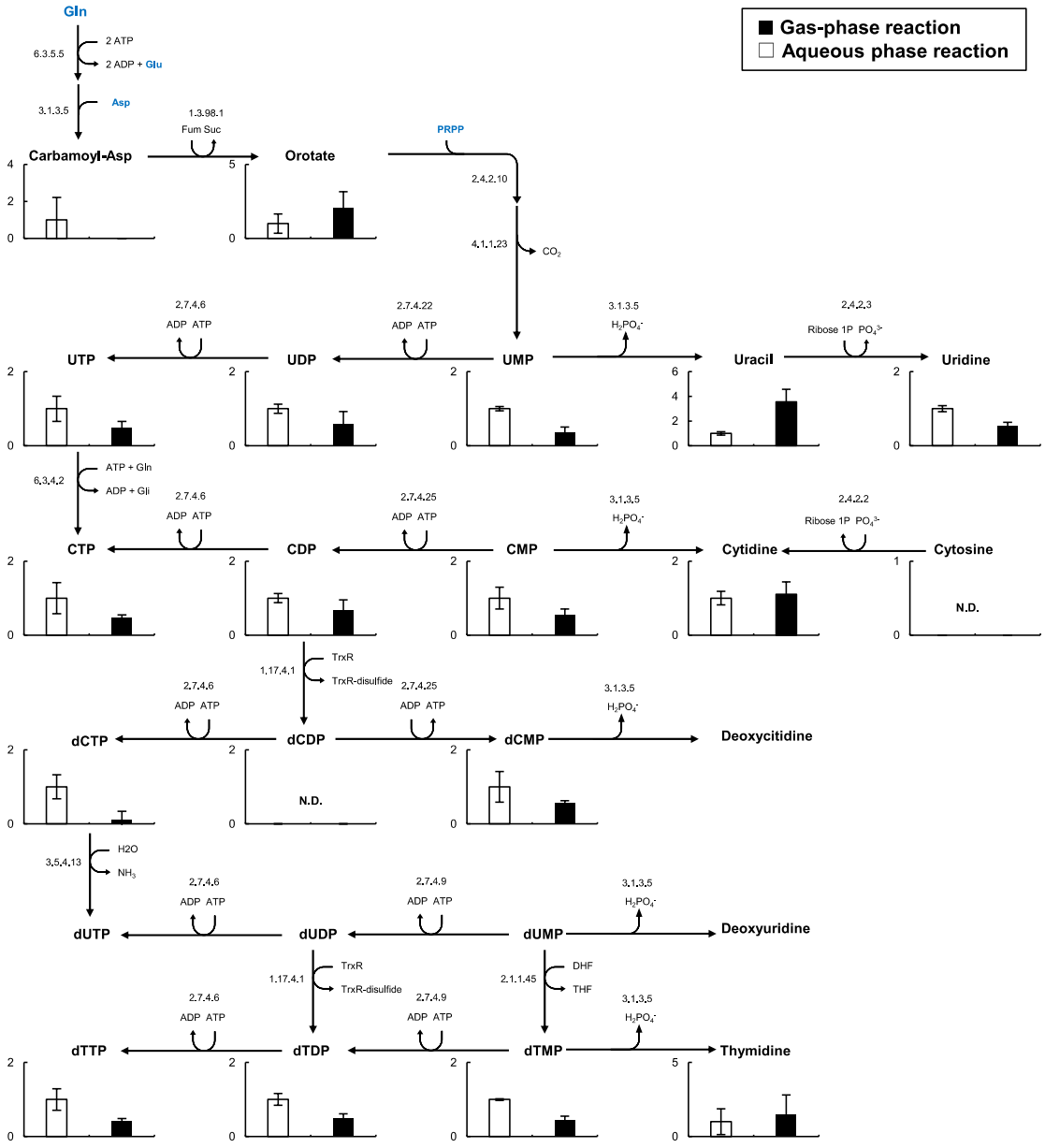

Fig. 6. Altered accumulation of metabolites involved in pyrimidine metabolism in cells in the gas-phase reaction. Each graph indicates the relative level of each intracellular metabolite normalized to the value in cells catalyzing the aqueous phase reaction for 3 h. Error bars show the standard deviation (n = 3).

Acknowledgements

This work was supported by the Advanced Low Carbon Technology Research and Development Program (JPMJAL1402 and JPMJAL1607) of the Japan Science and Technology Agency, the project JPNP18016 of the New Energy and Industrial Technology Development Organization, Japan, KAKENHI grants JP18K14065 and JP17H06304 from the Japan Society for the Promotion of Science, and the Cooperative Research Project Program of the Medical Institute of Bioregulation, Kyushu University.

Appendix A. Supplementary data

Supplementary data to this article can be found online at https://doi.org/10.1016/j.biortech.2021.125002.

References

Bjorck, C.E., Dobson, P.D., Pandhal, J., 2018. Biotechnological conversion of methane to methanol: evaluation of progress and potential. AIMS Bioeng. 5, 1–38.

Cantera, S., Bordel, S., Lebrero, R., Gancedo, J., Garcia-Encina, P.A., Munoz, R., 2019. Bio-conversion of methane into high profit margin compounds: an innovative, environmentally friendly and cost-effective platform for methane abatement. World J. Microbiol. Biotechnol. 35, 16.

Chen, H.-L., Bernard, C.S., Hubert, P., My, L., Zhang, C.-C., 2014. Fluorescence resonance energy transfer based on interaction of PII and PipX proteins provides a robust and specific biosensor for 2-oxoglutarate, a central metabolite and a signalling molecule. FEBS J. 281 (4), 1241–1255.

Chen, Y.-Y., Ishikawa, M., Suzuki, R., Ito, H., Kamachi, T., Hori, K., 2020. Evaluation of methane degradation performance in microbial gas-phase reactions using effectively immobilized methanotrophs. Biochem. Eng. J. 154, 107441.

Daniel, J., Danchin, A., 1986. 2-Ketoglutarate as a possible regulatory metabolite involved in cyclic AMP-dependent catabolite repression in *Escherichia coli* K12. Biochimie. 68 (2), 303–310.

David, F., Nielsen, J., Siewers, V., 2016. Flux control at the malonyl-CoA node through hierarchical dynamic pathway regulation in *Saccharomyces cerevisiae*. ACS Synth. Biol. 5 (3), 224–233.

Doucette, C.D., Schwab, D.J., Wingreen, N.S., Rabinowitz, J.D., 2011. α-ketoglutarate coordinates carbon and nitrogen utilization via enzyme I inhibition. Nat. Chem. Biol. 7 (12), 894–901.
Fei, Q., Guarnieri, M.T., Tao, L., Laurens, L.M.L., Dowe, N., Pienkos, P.T., 2014. Bioconversion of natural gas to liquid fuel: opportunities and challenges. Biotechnol. Adv. 32 (3), 596–614.
Furutani, M., Uenishi, A., Iwasa, K. 2014. Recombinant cell, and method for producing 1, 4-butanediol, Sekisui Chemical Co.
Fushimi, T., Izumi, Y., Takahashi, M., Hata, K., Murano, Y., Bamba, T., 2020. Dynamic metabolome analysis reveals the metabolic fate of medium-chain fatty acids in AML12 Cells. J. Agric. Food Chem. 68 (43), 11997–12010.
Ganendra, G., Mercado-Garcia, D., Hernandez-Sanabria, E., Boeckx, P., Ho, A., Boon, N., 2015. Methane biofiltration using autoclaved aerated concrete as the carrier material. Appl. Microbiol. Biotechnol. 99 (17), 7307–7320.
Gupta, A., Ahmad, A., Chothwe, D., Madhu, M.K., Srivastava, S., Sharma, V.K., 2019. Genome-scale metabolic reconstruction and metabolic versatility of an obligate methanotroph Methylococcus capsulatus str. Bath. PeerJ. 7, e6685.
Gupta, A., Reizman, I.M., Reisch, C.R., Prather, K.L., 2017. Dynamic regulation of metabolic flux in engineered bacteria using a pathway-independent quorum-sensing circuit. Nat. Biotechnol. 35, 273-279.
Huergo, L.F., Dixon, R., 2015. The emergence of 2-oxoglutarate as a master regulator metabolite. Microbiol. Mol. Biol. Rev. 79 (4), 419–435.
Izumi, Y., Matsuda, F., Hirayama, A., Ikeda, K., Kita, Y., Horie, K., Saigusa, D., Saito, K., Sawada, Y., Nakanishi, H., Okahashi, N., Takahashi, M., Nakao, M., Hata, K., Hoshi, Y., Morihara, M., Tanabe, K., Bamba, T., Oda, Y., 2019. Inter-laboratory comparison of metabolite measurements for metabolomics data integration. Metabolites. 9 (11), 257.
Jeon, Y.C., Nguyen, A.D., Lee, E.Y., 2019. Bioproduction of isoprenoids and other secondary metabolites using methanotrophic bacteria as an alternative microbial cell factory option: current stage and future aspects. Catalysts 9 (11), 883.
Kulishova, L.M., Zharkov, D.O., 2017. Solid/gas biocatalysis. Biochemistry (Moscow) 82 (2), 95–105.
Kumar, V., Ahluwalia, V., Saran, S., Kumar, J., Patel, A.K., Singhania, R.R., 2021. Recent developments on solid-state fermentation for production of microbial secondary metabolites: challenges and solutions. Bioresour. Technol. 323, 124566.
Lamare, S., Legoy, M.-D., Graber, M., 2004. Solid/gas bioreactors: powerful tools for fundamental research and efficient technology for industrial applications. Green Chem. 6 (9), 445.
Lee, O.K., Hur, D.H., Nguyen, D.T.N., Lee, E.Y., 2016. Metabolic engineering of methanotrophs and its application to production of chemicals and biofuels from methane. Biofuels. Bioprod. Biorefin. 10 (6), 848–863.
Liu, M., Fu, Y., Gao, W., Xian, M.o., Zhao, G., 2020. Highly efficient biosynthesis of hypoxanthine in *Escherichia coli* and transcriptome-based analysis of the purine metabolism. ACS Synth. Biol. 9 (3), 525–535.
McKeague, M., Wang, Y.-H., Cravens, A., Win, M.N., Smolke, C.D., 2016. Engineering a microbial platform for de novo biosynthesis of diverse methylxanthines. Metab. Eng. 38, 191–203.
Park, S., Lee, C.-H., Ryu, C.-R., Sung, K., 2009. Biofiltration for reducing methane emissions from modern sanitary landfills at the low methane generation stage. Water, Air, Soil Pollut. 196 (1-4), 19–27.
Patel, S.K.S., Kalia, V.C., Joo, J.B., Kang, Y.C., Lee, J.-K., 2020a. Biotransformation of methane into methanol by methanotrophs immobilized on coconut coir. Bioresour. Technol. 297, 122433.
Patel, S.K.S., Shanmugam, R., Kalia, V.C., Lee, J.-K., 2020b. Methanol production by polymer-encapsulated methanotrophs from simulated biogas in the presence of methane vector. Bioresour. Technol. 304, 123022.
Petersen, L.A.H., Villadsen, J., Jørgensen, S.B., Gernaey, K.V., 2017. Mixing and mass transfer in a pilot scale U-loop bioreactor. Biotechnol. Bioeng. 114 (2), 344–354.
Pieja, A.J., Rostkowski, K.H., Criddle, C.S., 2011. Distribution and selection of poly-3-hydroxybutyrate production capacity in methanotrophic proteobacteria. Microb. Ecol. 62 (3), 564–573.
Rabinowitz, J.D., Silhavy, T.J., 2013. Systems biology: metabolite turns master regulator. Nature. 500 (7462), 283–284.
Soma, Y., Fujiwara, Y., Nakagawa, T., Tsuruno, K., Hanai, T., 2017. Reconstruction of a metabolic regulatory network in *Escherichia coli* for purposeful switching from cell growth mode to production mode in direct GABA fermentation from glucose. Metab. Eng. 43, 54–63.
Soma, Y., Hanai, T., 2015. Self-induced metabolic state switching by a tunable cell density sensor for microbial isopropanol production. Metab. Eng. 30, 7–15.
Soma, Y., Tsuruno, K., Wada, M., Yokota, A., Hanai, T., 2014. Metabolic flux redirection from a central metabolic pathway toward a synthetic pathway using a metabolic toggle switch. Metab. Eng. 23, 175–184.
Strong, P.J., Kalyuzhnaya, M., Silverman, J., Clarke, W.P., 2016. A methanotroph-based biorefinery: potential scenarios for generating multiple products from a single fermentation. Bioresour. Technol. 215, 314–323.
Subbian, E. 2017. Production of lactic acid from organic waste or biogas or methane using recombinant methanotrophic bacteria, String Bio Private Limited.
Usami, A., Ishikawa, M., Hori, K., 2020. Gas-phase bioproduction of a high-value-added monoterpenoid (E)-geranic acid by metabolically engineered *Acinetobacter* sp. Tol 5. Green Chem. 22 (4), 1258–1268.
Wang, V.-C., Maji, S., Chen, P.-Y., Lee, H.K., Yu, S.-F., Chan, S.I., 2017. Alkane oxidation: methane monooxygenases, related enzymes, and their biomimetics. Chem. Rev. 117 (13), 8574–8621.
Ward, N., Larsen, Ø., Sakwa, J., Bruseth, L., Khouri, H., Durkin, A.S., Dimitrov, G., Jiang, L., Scanlan, D., Kang, K.H., Lewis, M., Nelson, K.E., Methé, B., Wu, M., Heidelberg, J.F., Paulsen, I.T., Fouts, D., Ravel, J., Tettelin, H., Ren, Q., Read, T., DeBoy, R.T., Seshadri, R., Salzberg, S.L., Jensen, H.B., Birkeland, N.K., Nelson, W.C., Dodson, R.J., Grindhaug, S.H., Holt, I., Eidhammer, I., Jonasen, I., Vanaken, S., Utterback, T., Feldblyum, T.V., Fraser, C.M., Lillehaug, J.R., Eisen, J.A., 2004. Genomic insights into methanotrophy: the complete genome sequence of *Methylococcus capsulatus* (Bath). PLoS Biol. 2 (10), e303.
Webb, C., 2017. Design aspects of solid state fermentation as applied to microbial bioprocessing. J. Appl. Biotechnol. Bioeng. 4, 511–532.
You, C., Okano, H., Hui, S., Zhang, Z., Kim, M., Gunderson, C.W., Wang, Y.-P., Lenz, P., Yan, D., Hwa, T., 2013. Coordination of bacterial proteome with metabolism by cyclic AMP signalling. Nature 500 (7462), 301–306.
Zha, X., Tsapekos, P., Zhu, X., Khoshnevisan, B., Lu, X., Angelidaki, I., 2021. Bioconversion of wastewater to single cell protein by methanotrophic bacteria. Bioresour. Technol. 320, 124351.
Zhang, C., Wei, Z.-H., Ye, B.-C., 2013. Quantitative monitoring of 2-oxoglutarate in *Escherichia coli* cells by a fluorescence resonance energy transfer-based biosensor. Appl. Microbiol. Biotechnol. 97 (18), 8307–8316.
Zhang, C., Ye, B.-C., 2014. A single fluorescent protein-based sensor for in vivo 2-oxo-gluatarate detection in cell. Biosens. Bioelectron. 54, 15–19.
Zhao, E.M., Zhang, Y., Mehl, J., Park, H., Lalwani, M.A., Toettcher, J.E., Avalos, J.L., 2018. Optogenetic regulation of engineered cellular metabolism for microbial chemical production. Nature 555 (7698), 683–687.